Tellus
SERIES A
DYNAMIC
METEOROLOGY
AND OCEANOGRAPHY
PUBLISHED BY THE INTERNATIONAL METEOROLOGICAL INSTITUTE IN STOCKHOLM

Tellus (2009), 61A, 587–600
Printed in Singapore. All rights reserved

TELLUS

The maximum likelihood ensemble filter performances in chaotic systems

By ALBERTO CARRASSI[1]*, STEPHANE VANNITSEM[1], DUSANKA ZUPANSKI[2] and MILIJA ZUPANSKI[2], [1]*Institut Royal Météorologique de Belgique, Av. Circulaire 3, 1180 Brussels, Belgium;* [2]*Cooperative Institute for Research in the Atmosphere, Colorado State University, Fort Collins, CO, USA*

(Manuscript received 9 January 2009; in final form 3 June 2009)

ABSTRACT

The performance of the maximum likelihood ensemble filter (MLEF), is investigated in the context of generic systems featuring the essential ingredients of unstable dynamics and on a spatially extended system displaying chaos. The main objective is to clarify the response of the filter to different regimes of motion and highlighting features which may help its optimization in more realistic applications. It is found that, in view of the minimization procedure involved in the filter analysis update, the algorithm provides accurate estimates even in the presence of prominent non-linearities. Most importantly, the filter ensemble size can be designed in connection to the properties of the system attractor (Kaplan–Yorke dimension), thus facilitating the filter setup and limiting the computational cost by using an optimal ensemble. As a corollary, this latter finding indicates that the ensemble perturbations in the MLEF reflect the intrinsic system error dynamics rather than a sampling of realizations of an unknown error covariance.

1. Introduction

In physics, engineering and natural sciences in general, one is typically interested in estimating the state of an evolving system for either diagnostic or prediction purposes. The problem consists in practice in determining as accurately as possible the system's state from sparse and noisy information sources. In the context of the classical estimation and control theories, a number of data assimilation algorithms have been proposed depending on the type of the systems and/or on the properties of the observations at disposal. It is well recognized how the classical Kalman filter (KF) for linear systems has represented a fundamental source of inspiration as well as an useful mathematical framework for the development of advanced data assimilation techniques applied to complex non-linear dynamics (Kalman, 1960). Along this line the data assimilation for numerical weather prediction (NWP), and for environmental prediction in general, has so far represented a stimulating field of applications giving up to a flourishing of advancements in the methodologies. The positive impact of the implementation of progressively more advanced assimilation methods on the overall accuracy of the present global weather predictions is well recognized.

When faced to state estimation for systems describing some natural phenomena, one fundamental obstacle is represented by the chaotic behaviour affecting most of realistic systems. The chaotic property undoubtedly most relevant for the data assimilation is the sensitivity to initial conditions which implies a rapid growth of the errors. This problem is at the origin of the efforts made in recent years to supply data assimilation algorithms with accurate descriptions of the uncertainty associated to the state estimate. The so called ensemble based data assimilation algorithms address this problem, giving a time-dependent description of the errors by means of an evolving ensemble of trajectories. A pioneering contribution was the introduction of a Monte Carlo approach referred to as ensemble Kalman filter (EnKF; Evensen, 1994). The research in the field has thereafter experienced a strong activity through the introduction of a number of EnKF-inspired techniques and of the complementary class of algorithms known as reduced rank square-root filters (Houtekamer and Mitchell, 1998; Anderson, 2001; Bishop et al., 2001; Heemink et al., 2001; Whitaker and Hamill, 2002; Ott et al., 2004). Most of these methodologies, as well as the original KF, follow a minimum variance approach to obtain the state best estimate, the analysis. With the goal of their implementation in operational NWP models, these algorithms have been also applied to chaotic systems although the relation between their performances and the dynamical properties of the

*Corresponding author.
e-mail: a.carrassi@oma.be
DOI: 10.1111/j.1600-0870.2009.00408.x

system at hand, was not necessarily the central concern. In a recent work, for instance, the differences between the Monte Carlo based (also referred to as stochastic) and the square-root (also referred to as deterministic) filters have been analysed with an emphasis on the filter response to the system non-linearities, inducing non-Gaussian error distributions (Lawson and Hansen, 2004). Other interesting questions such as the design of efficient observational deployments (Ghil, 1997) and the development of data assimilation methods explicitly aimed at controlling system instabilities (Trevisan and Uboldi, 2004), were also treated in the light of chaos theory.

The maximum likelihood ensemble filter (MLEF) is an ensemble data assimilation technique based on control theory (Zupanski, 2005; Zupanski and Zupanski, 2006). The analysis in the MLEF is obtained as the maximum of the probability density function (PDF), determined through an iterative minimization of a cost-function derived from a multivariate a posteriori PDF. For non-linear, and possibly chaotic, systems this procedure provides a practical way of finding the non-linear analysis solution. The MLEF has been successfully applied to various models, such as the Korteweg-de Vries-Burgers equation (Zupanski, 2005; Zupanski and Zupanski, 2006), the Colorado State University (CSU) global shallow-water model (Zupanski et al., 2006; Uzunoglu et al., 2007), the Large-Eddy simulation model (Carrio et al., 2008), the National Aeronautics and Space Administration GEOS-5 column precipitation model (Zupanski et al., 2007a), and the CSU Lagrangian Particle Dispersion Model (Zupanski et al., 2007b).

Despite of this trend of success, the lack of a focused analysis on the MLEF performance in the context of chaotic dynamics, is the motivation of the present study. In an effort to understand if the algorithm's setup optimization can be designed in relation to the intrinsic stability properties of the dynamics, the essential features of the MLEF procedure are thus revisited. Studying the response of the filter in a range of different regimes of motion should help identifying the potential advantages and drawbacks of the algorithm, as well as guiding its future implementations to this class of systems. In particular, emphasis is placed on the design of an adequate ensemble's size in connection to the properties of the system dynamics. Prototypical systems, simple enough to allow for the derivation of the filter analytical solution are first analysed. A detailed numerical analysis is then performed for a spatially extended system displaying chaos.

The paper is organized as follows. In the first part of Section 2 the formulation of the MLEF is summarized, while a preliminary discussion on the impact of chaotic dynamics is drawn in the second part of the section. In Section 3, results from a scalar and a bi-dimensional unstable dynamics are described, while Section 4 contains results from the numerical analysis in the case of a spatially extended system whose parameters are changed in order to simulate a wide range of motions, from periodic to highly chaotic. Conclusion are then given in Section 5.

2. Maximum likelihood ensemble filter

2.1. Formulation

In this section, we provide a review of the MLEF formulation, following closely the description given in Zupanski et al. (2008).

Let S denote the I-dimensional system's phase space and $\mathbf{x}$ the state vector of dimension I. Accordingly, the set of N state vectors constituting the ensemble is defined as $\{\mathbf{x}_i, i = 1, \ldots, N\}$, and the ensemble subspace as E.

The MLEF analysis cycle initialization needs the specification of both the initial state estimate, $\mathbf{x}(t_0) = \mathbf{x}^0$, and the associated uncertainty (in terms of an error covariance), $\mathbf{P}^0$. In the present formulation the dynamical model is assumed to be perfect. Initial perturbations to the reference trajectory $\mathbf{x}^0$, $\{\mathbf{p}_i^0, i = 1, \ldots, N\}$, are used to define the error covariance, as the columns of an $I \times N$ square-root error covariance at the initial time.

The initial state vector and the initial square-root error covariance define the set of N initial conditions $\mathbf{x}_i^0 = \mathbf{x}^0 + \mathbf{p}_i^0$, $i = 1, \ldots, N$, from which N analysis cycles start. Let us consider a (usually non-linear and dissipative) prediction model expressed as a discrete time mapping

$$\mathbf{x}_{t+1} = \mathcal{M}(\mathbf{x}_t), \tag{1}$$

t being the time. The dynamical model $\mathcal{M}$ is used to obtain both the system state prediction (the forecast) from a previous analysis

$$\mathbf{x}^f = \mathcal{M}(\mathbf{x}^a), \tag{2}$$

where the f and a stand for forecast and analysis, respectively (time index has been omitted for simplicity), and to propagate in time the error covariance. Let the set of N analysis perturbations to the analysis state at an arbitrary analysis time, be denoted by $\{\mathbf{p}_i^a, i = 1, \ldots, N\}$; they enter the columns of the square-root, $I \times N$ analysis error covariance matrix $\mathbf{P}_a^{1/2}$. Now these analysis perturbations define a set of initial conditions for the subsequent prediction step; the ith forecast perturbation resulting from the evolution of the ith analysis perturbation is

$$\mathbf{p}_i^f = \mathcal{M}\left(\mathbf{x}_i^a\right) - \mathcal{M}(\mathbf{x}^a) = \mathcal{M}\left(\mathbf{x}^a + \mathbf{p}_i^a\right) - \mathcal{M}(\mathbf{x}^a) \tag{3}$$

and $\{\mathbf{p}_i^f, i = 1, \ldots, N\}$ represent the columns of the square-root forecast error covariance matrix $\mathbf{P}_f^{1/2}$.

The MLEF operates as a sequential assimilation scheme, updating the state estimate at a given time when observations are available. The analysis solution is obtained following a maximum likelihood approach, which implies that the analysis is imposed to be the state which maximizes the posterior probability distribution. As in the three-dimensional variational assimilation (Lorenc, 1986), this is pursued by minimizing a scalar, non-linear, cost-function $J(\mathbf{x})$ measuring the data-to-model misfit.

Assuming Gaussian error distributions, $J(\mathbf{x})$ can be written as

$$2J(\mathbf{x}) = (\mathbf{x} - \mathbf{x}^f)^T \mathbf{P}_f^{-1} (\mathbf{x} - \mathbf{x}^f) + [\mathbf{y} - \mathcal{H}(\mathbf{x}^f)]^T \mathbf{R}^{-1} [\mathbf{y} - \mathcal{H}(\mathbf{x}^f)], \quad (4)$$

where $\mathbf{y}$ represents the M-dimensional observational vector, $\mathbf{R}$ the $M \times M$ observation error covariance matrix and $\mathcal{H}$ the observation operator mapping from model to observation space.

Since the forecast error covariance matrix is defined using the ensemble, $\mathbf{P}_f = \mathbf{P}_f^{1/2} (\mathbf{P}_f^{1/2})^T$, no matter the specific algorithm used to minimize (4), the analysis increment will span the ensemble of forecast perturbations, so that $\Delta \mathbf{x}^a = (\mathbf{x}^a - \mathbf{x}^f) \in A = span\{\mathbf{p}_1^f, \mathbf{p}_2^f, \ldots, \mathbf{p}_N^f\}$; note that $A \subset S$ and $\mathbf{P}_f^{1/2} : E \rightarrow \mathrm{A}$. This means that the analysis increment will be a linear combination of the forecast ensemble perturbations $\mathbf{p}_i^f$, and that the coefficients vector for this combination, $\mathbf{w}$, is in the ensemble space. In practice $\Delta \mathbf{x}^a = \mathbf{P}_f^{1/2} \mathbf{w}$ and the matrix $\mathbf{P}_f^{1/2}$ acts as a projection operator. Thus, the minimization can be done efficiently in the ensemble subspace.

In the present application a preconditioned non-linear conjugate gradient method is used and the variable transformation is defined following a generalized Hessian approach. The important aspect is that, since the subspace A, where the analysis increment is confined, is automatically defined by the ensemble, in deriving the derivative of the cost-function, only increments in the space A are considered, so that the cost-function gradient is an N-dimensional vector, while its Hessian a $N \times N$ matrix. The control variable precondition in the space spanned by the ensemble A reads $\mathbf{w} = [\nabla^2 J(\mathbf{x}^f)]^{-1/2} \xi$, ξ being the N-dimensional control variable for the minimization. Finally, the analysis increment in the whole system's phase space is derived

$$\Delta \mathbf{x}_a = \mathbf{P}_f^{1/2} [\nabla^2 J(\mathbf{x}^f)]^{-1/2} \xi. \quad (5)$$

Note that the Hessian matrix is evaluated at the forecast field $\mathbf{x}^f$.

As shown in Zupanski (2005), the Hessian matrix is equal to

$$\nabla^2 J(\mathbf{x}^f) = (\mathbf{I} + \mathbf{C})^T, \quad (6)$$

where $\mathbf{C}$ is a $N \times N$ symmetric positive definite matrix given by

$$\mathbf{C} = \mathbf{Z}^T \mathbf{Z}. \quad (7)$$

The practical problem of determining $\mathbf{C}$ is overcome by exploiting the forecast ensemble. As shown in Zupanski (2005) in fact, the i^{th} column of $\mathbf{Z}$ is given by $\mathbf{z}_i = \mathbf{R}^{-1/2} \mathcal{H}(\mathbf{x} + \mathbf{p}_i^f) - \mathbf{R}^{-1/2} \mathcal{H}(\mathbf{x})$.

Once the matrix $\mathbf{C}$ is evaluated, the square-root and inversion involved in the variable transformation for the precondition (5)–(6) is done through the eigenvalue decomposition (EVD) of $\mathbf{C}$. Assuming $\mathbf{V}$ and $\mathbf{\Gamma}$ are the eigenvectors and the eigenvalue matrices, respectively, we have $\mathbf{C} = \mathbf{V} \mathbf{\Gamma} \mathbf{V}^T$ and $(\mathbf{I} + \mathbf{C})^{-T/2} = \mathbf{V} (\mathbf{I} + \mathbf{\Gamma})^{-1/2} \mathbf{V}^T$. Now all the entries for the control variable precondition are determined. Finally, the cost-function minimization is performed by exploiting the gradient in the ensemble subspace within a conjugate gradient method. Full details on the MLEF procedure can be found in Zupanski (2005) and Zupanski et al. (2008).

The update of the analysis error covariance completes the analysis step. This is done by directly transforming the square-root of the ensemble based forecast error covariance matrix, into the analysis one, according to

$$\mathbf{P}_a^{1/2} = \mathbf{P}_f^{1/2} [\mathbf{I} + \mathbf{C}(\mathbf{x}_{\text{opt}})]^{-T/2}, \quad (8)$$

where $\mathbf{x}_{\text{opt}}$ indicates the optimized analysis. The columns of $\mathbf{P}_a^{1/2}$ are then used as the initial perturbations for the next analysis cycle, and the entire procedure can be repeated.

Note that a distinctive feature of the MLEF (with respect to either deterministic or stochastic filters) is that there is no explicit normalization in the ensemble based forecast covariance evaluation. Usually, the spread of the forecast ensemble is normalized with the size of the ensemble itself. In a number of cases, among which the EnKF, this choice allows to write the filter equations in a closed form whose solution, for a linear system, has the attractive feature of converging to the standard KF solution in the limit of an infinite number of ensemble members. The justification for not normalizing the forecast error covariance comes from the link between the MLEF and the KF. This link also applies to the SEEK filter (Pham et al., 1998; Rozier et al., 2007). In practice, in the MLEF the normalization of the forecast error covariance is substituted by normalization of the analysis error covariance at the previous analysis time.

To explain this difference, let us consider the linear case with the model indicated by the operator $\mathbf{M}$. We can write for the mean $\mathbf{x}^f = \mathbf{M}\mathbf{x}^a$ and for the ensemble members $\mathbf{x}_i^f = \mathbf{M}\mathbf{x}_i^a$, $i = 1, \ldots, N$. By performing the difference $\mathbf{x}^f - \mathbf{x}_i^f = \mathbf{M}\mathbf{x}^a - \mathbf{M}\mathbf{x}_i^a = \mathbf{M}(\mathbf{x}^a - \mathbf{x}_i^a)$, and using $\mathbf{P}^f = \langle (\mathbf{x}^f - \mathbf{x}_i^f)(\mathbf{x}^f - \mathbf{x}_i^f)^T \rangle$, where $\langle\,\rangle$ is the expectation, the forecast error covariance can be written in two ways

$$\mathbf{P}^f = \left\langle \left[\mathbf{M}\left(\mathbf{x}^a - \mathbf{x}_i^a\right)\right] \left[\mathbf{M}\left(\mathbf{x}^a - \mathbf{x}_i^a\right)\right]^T \right\rangle = \frac{1}{N-1} \sum_{i=1}^{N} \left[\mathbf{M}\left(\mathbf{x}^a - \mathbf{x}_i^a\right)\right] \left[\mathbf{M}\left(\mathbf{x}^a - \mathbf{x}_i^a\right)\right]^T \quad (9)$$

$$\mathbf{P}^f = \mathbf{M} \left\langle \left(\mathbf{x}^a - \mathbf{x}_i^a\right) \left(\mathbf{x}^a - \mathbf{x}_i^a\right)^T \right\rangle \mathbf{M}^T = \mathbf{M}\mathbf{P}^a\mathbf{M}^T. \quad (10)$$

Formulations (9) and (10) are equivalent for linear model $\mathbf{M}$ and are used here only to clarify the reason for (not) normalizing $\mathbf{P}^f$ in the MLEF. The formulation (9) is used in the Monte Carlo-based filters (e.g. EnKF), while the formulation (10) corresponds to the KF-based filters (e.g. MLEF, SEEK). In (9), the perturbations (without any normalization) are used at the initial time of model integration. Therefore, normalization is required at the end time of the forecast, as it is done in the EnKF. In (10), the initial perturbations are the columns of the square-root analysis error covariance, which is normalized as in (8). Although the normalization procedure differs in various methods (MLEF uses an inverse Hessian as an approximation for analysis

error covariance), the point is that normalization is done at the analysis step, that is at the initial time of model integration. This is shown explicitly in the analysis of the MLEF equations provided in Section 3.

2.2. MLEF and chaotic dynamics

The application to non-linear chaotic dynamics constitutes an useful challenge for a state-estimation technique. In this section we draw some conjectures on how chaotic behaviour and system instabilities may impact the MLEF performance and eventually modify the filter setup for the applications to this class of systems.

The MLEF can be seen as a hybrid data assimilation scheme. By construction, it shares features coming from both variational and ensemble based schemes (Zupanski, 2005). A distinction is typically done between deterministic and stochastic ensemble filters (see e.g. Tippet et al., 2003, and references therein). The essential feature which makes this distinction, and which is also relevant for our discussion, is that, while in stochastic filters (i.e. the EnKF) each ensemble trajectory undergoes an independent analysis update in which a different set of observations is assimilated, in deterministic filters the updated analysis ensemble is obtained through a linear transformation (usually under the matrix form) applied to the forecast ensemble. This transformation matrix, $\mathbf{T}$, is usually defined under the constraint that the updated analysis error covariance matches a desired value such as, for instance, that predicted by the extended Kalman filter (EKF). Posed in this form, the solution (a square-root matrix) is not unique and the particular choice employed characterizes the filter algorithm (Tippet et al., 2003). The difference in the analysis ensemble update between stochastic and deterministic filters has important implications, and lead to remarkable differences in the filter response to non-Gaussian error distributions (Lawson and Hansen, 2004). This is a main concern for the applications to chaotic dynamics where the instabilities may rapidly drive the error PDF out from Gaussianity.

In the MLEF the update of the analysis ensemble members is made through the direct transformation of the forecast ensemble (8). In contrast to deterministic filters, and in agreement with the MLEF maximum likelihood approach, this transformation is obtained by imposing that the resulting analysis error covariance matrix is equal to the inverse of the Hessian matrix of the cost-function evaluated at the minimum (Zupanski, 2005). As a consequence, the properties of the analysis-forecast ensemble transformation are connected to those of the observation operator (which enters the dependence of the analysis on the forecast field). If the latter is linear, the MLEF analysis solution is obtained in a single step of minimization iteration and the transformation $\mathbf{T} = (\mathbf{I} + \mathbf{C})^{-T/2}$ is linear as for deterministic filters. In the case of non-linear observation operator, on the other hand, the MLEF could have several iterations of minimization, which would produce a non-linear relationship between the analysis and the forecast (first guess) state, which in turn would imply a non-linear relationship between the analysis and the forecast ensemble (see Zupanski, 2005, for an application with a quadratic observation operator). We can thus argue that, at least in the case of linear observation operators, the MLEF ensemble update will resemble that of deterministic filters.

On the other hand, since the MLEF analysis solution is obtained via the minimization of a cost-function, the MLEF does not seek the maximum likelihood solution as an approximation of the EKF one, or some other linear update, but it just calculates the first mode of a posteriori PDF which coincides with the mean for Gaussian PDF. This may improve the accuracy of the state estimation in the presence of strong non-linearities. Nevertheless, unless non-Gaussian distributions are explicitly taken into account in the cost-function formulation, the updated analysis uncertainty is anyhow given by a Gaussian PDF. As shown in Fletcher and Zupanski (2006a,b, 2008) the MLEF produces a different solution for non-Gaussian PDFs.

The way the ensemble information content is used and spread out all over the model domain at the MLEF analysis step, is ultimately related to the matrix $\mathbf{C}$; the latter has been also referred to as 'information matrix in ensemble subspace' as it allows for a connection between information theory and ensemble data assimilation (Zupanski et al., 2007a). Through $\mathbf{P}_f^{1/2}$ the matrix $\mathbf{C}$ is directly connected to the dynamics so that its properties are expected to have a dependence on the regimes of motion. The matrix $\mathbf{C}$ is of order $N \times N$, symmetric, and positive definite. Its possible maximum rank is given by the smaller number between N and M (assuming that the rank of $\mathbf{R}$ coincides with M, its order, which is the case, for instance, for uncorrelated observations); $M \gg N$ in typical atmospheric and oceanic applications. In practice, the rank properties of $\mathbf{C}$ are indicative of the two competitive factors entering the estimation problem: the number of independent phase space directions where forecast error is estimated to be grown, as represented by the rank of $\mathbf{P}_f^{1/2}$, and the amount of information at disposal, as represented by the rank of $\mathbf{R}$. Chaotic motion will directly affect the rank of $\mathbf{P}_f^{1/2}$, eventually reducing it as a consequence of the error dynamics confinement characteristic of these systems. This circumstance is typical in data assimilation for chaotic dynamics where, in virtue of this error confinement, an efficient control of the error growth can, under certain conditions, be obtained by assimilating only a limited amount of observations, whose number is connected to the number of relevant error growing directions (Carrassi et al., 2008a). This suggests that, for this kind of systems, to adequately explain the actual error variance, the MLEF ensemble size should be adjusted in the light of the system dynamical properties.

3. Prototypical systems

In this section, the full MLEF filter procedure is derived for two generic unstable systems which are simple enough to allow

for the analytical deduction of the analysis state and covariance updates.

3.1. Linear scalar system

We consider first the simple case of a scalar and linear dynamical system given by the ordinary differential equation:

$$\frac{\mathrm{d}x}{\mathrm{d}t} = \lambda x. \tag{11}$$

The system has an equilibrium point at the origin, which is unstable for $\lambda > 0$. We are interested in studying the dynamics around this unstable point. Furthermore, let us assume that a noisy observation x_o, with error standard deviation σ_o, is available every $t = \tau$ and that only one ensemble member is employed. The MLEF analysis state and variance updates then read

$$x_a(t) = \frac{x_f(t) + x_\mathrm{o}\dfrac{\sigma_f^2(t)}{\sigma_\mathrm{o}^2}}{1 + \dfrac{\sigma_f^2(t)}{\sigma_\mathrm{o}^2}} \tag{12}$$

$$\sigma_a^2(t) = \frac{\sigma_f^2(t)}{1 + \dfrac{\sigma_f^2(t)}{\sigma_\mathrm{o}^2}} \tag{13}$$

with $\sigma_f(t) = \sigma_a(t-\tau)\,\mathrm{e}^{\lambda\tau}$ and $x_f(t) = x_a(t-\tau)\,\mathrm{e}^{\lambda\tau}$. Note that the equations are equivalent to the classical KF equations for a scalar system. The error doubling time, T_2, is related to the model parameter λ through $T_2 = \ln 2/\lambda$. As usual, a relevant parameter which helps understanding and generalizing results is the ratio between the assimilation interval τ and the error doubling time. The latter is estimated equal to 2 d in operational weather prediction models (Kalnay, 2003) which are typically run in assimilation cycles with $6 \le \tau \le 12$ h, that is $(1/8)T_2 \le \tau \le (1/4)T_2$. In the toy system (11), with $\lambda = 0.5$, the same conditions are reproduced by choosing τ smaller than about 0.34.

In the case of an ensemble of size 2, the update equations read

$$x_a(t) = \frac{x_f(t) + x_\mathrm{o}\dfrac{\sigma_{f,1}^2(t) + \sigma_{f,2}^2(t)}{\sigma_\mathrm{o}^2}}{1 + \dfrac{\sigma_{f,1}^2(t) + \sigma_{f,2}^2(t)}{\sigma_\mathrm{o}^2}} \tag{14}$$

for the state update, and

$$\sigma_{a,1}^2(t) = \frac{\sigma_{f,1}^2(t)}{1 + \dfrac{\sigma_{f,1}^2(t) + \sigma_{f,2}^2(t)}{\sigma_\mathrm{o}^2}}$$

$$\sigma_{a,2}^2(t) = \frac{\sigma_{f,2}^2(t)}{1 + \dfrac{\sigma_{f,1}^2(t) + \sigma_{f,2}^2(t)}{\sigma_\mathrm{o}^2}} \tag{15}$$

for the variances update. The forecast error variance evolution is given by $\sigma_{f,1}^2(t) = \sigma_{a,1}^2(t-\tau)\,\mathrm{e}^{2\lambda\tau}$ and $\sigma_{f,2}^2(t) = \sigma_{a,2}^2(t-\tau)\,\mathrm{e}^{2\lambda\tau}$ for each member, respectively, and $x_f(t) = x_a(t-\tau)\mathrm{e}^{\lambda\tau}$. Note that $N > I$ in this case.

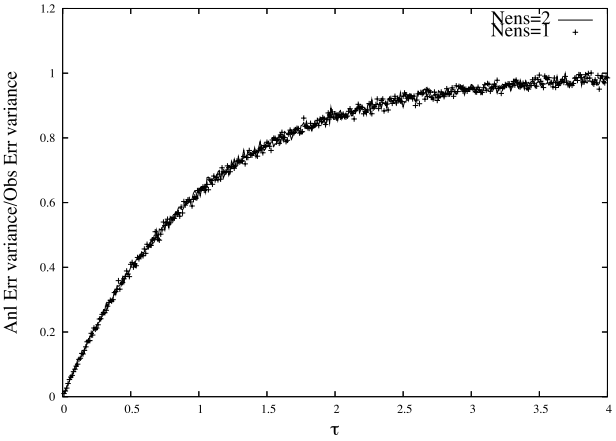

Fig. 1. Scalar unstable dynamics. Mean analysis error variance, normalized with respect to the observation error as a function of the assimilation interval τ. Single member ensemble (pluses); two member ensemble (line).

A comparison between the update eqs. (12) and (13) for the single member case, with (14) and (15) of the two members ensemble, immediately reveals their formal equivalence, with the exception that in the last case the forecast error variance σ_f^2 is replaced with the combined contribution of the two members, $\sigma_{f,1}^2 + \sigma_{f,2}^2$. The increase of the variance estimated by the ensemble is compensated by an implicit renormalization at the analysis step during which $\sigma_{a,1}^2$ and $\sigma_{a,2}^2$ are updated through a weighting by the inverse of the global error variance of the ensemble. Figure 1 shows the variation of the mean analysis error variance, normalized with respect to the observation error variance, as a function of the assimilation interval τ for two set of experiments with one and two members, respectively. The results are obtained over a sample of 10^5 analysis cycles.

For all the value of τ considered an improvement with respect to the observation error is obtained, but the analysis accuracy get progressively worse for larger values of τ. Note that if $\lambda < 0$, the analysis error variance will converge to zero, at a rate related to $|\lambda|$, and the assimilation of observations will become formally useless. We point out that this conclusion holds only for an asymptotic analysis as the one undergone here; even for stable systems the assimilation of observations may be beneficial during a transient period. Nevertheless, the key aspect here is the lack of any benefit when the ensemble size passes from one to two members. Therefore, our preliminary conclusion is that increasing the ensemble size beyond the system dimension does not provide improvements of the filter performance. Finally, note that for long time we have $\sigma_{f,1}^2 = \sigma_{f,2}^2 = 1/2(\sigma_f)^2$; in practice a process of 'energy distribution' occurs with the result that the weight of each of the two members in the estimate of the forecast error variance is equal, and that their sum is equal to σ_f^2 in the single member case.

3.2. Saddle node

The second prototype of unstable dynamics considered here is the saddle node, a two-dimensional non-linear dynamical system which can be written as

$$\frac{\mathrm{d}x_1}{\mathrm{d}t} = \alpha - x_1^2$$
$$\frac{\mathrm{d}x_2}{\mathrm{d}t} = -x_2. \tag{16}$$

For $\alpha > 0$, the system possess two equilibrium points, $(-\sqrt{\alpha}, 0)$ and $(\sqrt{\alpha}, 0)$, which are unstable and stable, respectively. As in the previous example we analyse the dynamics around the unstable equilibrium point; we assume therefore that the state we intend to estimate is $(-\sqrt{\alpha}, 0)$. This point is characterized by one unstable direction, along x_1, whose divergence rate is $|\lambda_1| = 2\sqrt{\alpha}$ and by one stable direction, along x_2, with a convergence rate $|\lambda_2| = 1$; note that in order to emulate a chaotic dissipative system α has to be set so that $-1 + 2\sqrt{\alpha} < 0$ which implies $0 < \alpha < 1/\sqrt{2}$.

We assume to observe the full system, $\mathbf{x}_\mathrm{o} = (x_{\mathrm{o},1}, x_{\mathrm{o},2})$, every $t = \tau$; the observation operator reduces to the 2×2 identity matrix. If a single member is used, one can analytically show that the MLEF analysis update reads

$$\begin{aligned} x_{a,1}(t) &= \left[1 - \frac{\sigma_{f,1}^2}{\sigma_{\mathrm{o},1}^2\beta}\right] x_{f,1}(t) - \frac{\sigma_{f,1}\sigma_{f,2}}{\sigma_{\mathrm{o},2}^2\beta} x_{f,2}(t) \\ &\quad + \frac{\sigma_{f,1}^2}{\sigma_{\mathrm{o},1}^2\beta} x_{\mathrm{o},1} + \frac{\sigma_{f,1}\sigma_{f,2}}{\sigma_{\mathrm{o},2}^2\beta} x_{\mathrm{o},2} \\ x_{a,2}(t) &= \left[1 - \frac{\sigma_{f,2}^2}{\sigma_{\mathrm{o},2}^2\beta}\right] x_{f,2}(t) - \frac{\sigma_{f,1}\sigma_{f,2}}{\sigma_{\mathrm{o},1}^2\beta} x_{f,1}(t) \\ &\quad + \frac{\sigma_{f,1}^2}{\sigma_{\mathrm{o},2}^2\beta} x_{\mathrm{o},2} + \frac{\sigma_{f,1}\sigma_{f,2}}{\sigma_{\mathrm{o},2}^2\beta} x_{\mathrm{o},1}, \end{aligned} \tag{17}$$

where $\beta = 1 + (\frac{\sigma_{f,1}}{\sigma_{\mathrm{o},1}})^2 + (\frac{\sigma_{f,2}}{\sigma_{\mathrm{o},2}})^2$. For the analysis variance update we have

$$\sigma_{a,1}^2 = \frac{\sigma_{f,1}^2}{\beta}$$
$$\sigma_{a,2}^2 = \frac{\sigma_{f,2}^2}{\beta}. \tag{18}$$

Note that the indexes refer here to the system components x_1 and x_2, respectively. The evolution of the forecast error variances within an assimilation interval is given by $\sigma_{f,1}^2(t) = \sigma_{a,1}^2(t - \tau)\mathrm{e}^{4\sqrt{\alpha}\tau}$ and $\sigma_{f,2}^2(t) = \sigma_{a,2}^2(t - \tau)\mathrm{e}^{-2\tau}$. In the case of an ensemble of two members, the derivation is a bit more involved and it is given in the Appendix. Note that in this case one must solve a linear system of two equations in order to get the optimal solutions in the space of the ensemble.

By inspecting eq. (17) we see that, for large τ (ideally tending to infinity), the first component of the analysis tends to the observation, as desired. On the other hand, and as a consequence of the stable character of the direction, the second component will tend to the forecast prediction (the truth) making the assimilation of observation along x_2 useless. In practice, observing the unstable direction only is sufficient to estimate the system's state. Note that these conclusions hold only in virtue of the dissipative character of the dynamics (as it is the case for any system describing some natural phenomena), which implies that the rate of convergence to the stable direction is larger than to the unstable one.

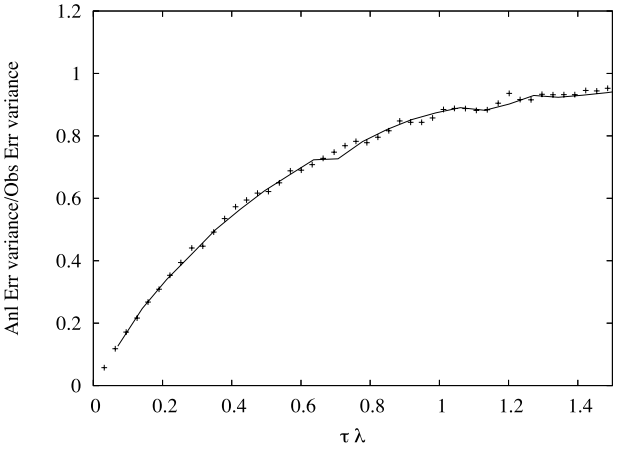

Fig. 2. Saddle point. Mean analysis error variance of the x-component, normalized with respect to the observation error along x, as a function of the adimensional factor $\lambda_1\tau$. $\lambda_1 = 2\sqrt{0.5}$ (line); $\lambda_1 = 2\sqrt{0.1}$ (pluses).

Figure 2 shows the results of experiments similar to those of Fig. 1. The analysis error variance of the x component, normalized with the observation error variance $\sigma_{\mathrm{o},1}^2$, is plotted here as a function of the adimensional factor $\lambda_1\tau$ and, as in the previous case, results are averaged over a large sample of initial conditions and after a transient period. The two curves refer to different choices of the parameter α, namely $\alpha = 0.1$ and 0.5. The convergence to the observation error for large τ is evident; in this situation the background is practically ignored and the assimilation is like a replacement. As expected, the convergence is more rapid in correspondence of the larger α, $\alpha = 0.5$, as it could be visualized by plotting the errors as a function of τ (not shown).

When a member is added to the ensemble, the filter response does not change significantly, as reported in Fig. 3 which shows the normalized analysis error variance along x_1 as a function of $\lambda_1\tau(\lambda_1 = 2\sqrt{0.5})$ for the experiments with one and two members ensemble, respectively. By observing that the two curves are very similar we conclude that the saturation of the filter performance with respect to the number of members, occurs for a value smaller than the system dimension (two in the present application).

Rather, this convergence appears related to the number of the unstable directions (one here). The figure reveals also that the filter with a two-dimensional ensemble size performs slightly worse than the single member case. This may be caused by

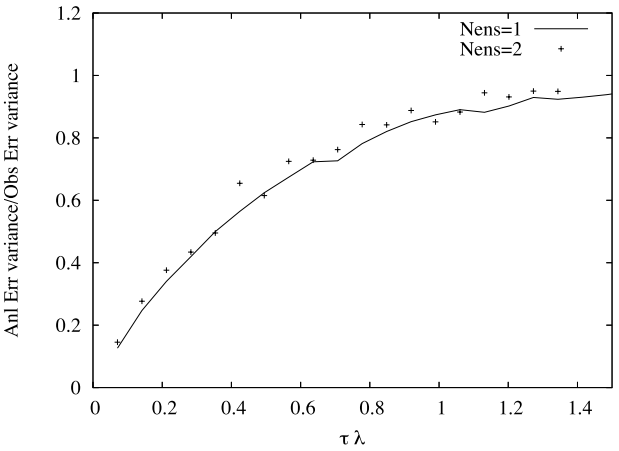

Fig. 3. Saddle point. Mean analysis error variance of the x_1-component, normalized with respect to the observation error along x_1, as a function of the adimensional factor $\lambda_1\tau$. Single member ensemble (line); two member ensemble (pluses).

the increase of numerical error when solving the linear system of equations of the MLEF algorithm; such errors are in fact expected to grow with the size of the ensemble. Another explanation can be given by invoking the role of the system's instabilities. The chances that, at the analysis time, the convergence of the members towards the unstable direction is not yet complete, are enhanced when larger ensembles are used. In that case, the ensemble members will still possess a non-vanishing component along the stable direction x_2. As a consequence, the analysis increment vector will also have a non-vanishing component along the same stable direction even if the projection of the actual error is negligible.

In summary, the results obtained in these two idealized systems allow us to conclude that, in the presence of unstable motion, the ensemble size in the MLEF should be chosen on the base of the number of system's unstable directions, instead on the full state dimension. This conclusion is valid in this idealized setting in which the unstable direction is fixed and unique. The application to complex realistic systems and/or systems subject to full chaotic dynamics can reveal more subtle relations as discussed in Section 4.

4. Numerical analysis

Let us now turn to a more complex example of unstable dynamics. The MLEF is studied now by performing observation system simulation experiments (OSSE) in the context of the spatially extended 36-variable dynamical system proposed by Lorenz (1995). The evolution equations read

$$\frac{\mathrm{d}x_i}{\mathrm{d}t} = (x_{i+1} - x_{i-2})x_{i-1} - x_i + F, \qquad i = \{1, \ldots, 36\}. \quad (19)$$

The quadratic term simulates the advection, the linear term the internal dissipation, while the constant term F plays the role of the external forcing. For a proper choice of the external forcing F, the model exhibits chaotic behaviour; a detailed description of the model can be found in Lorenz (1995). The numerical integrations here have been performed using a fourth-order Runge–Kutta scheme with a time step of 0.0083 units, corresponding to 1 hour of simulated time.

With the aim of simplifying the analysis and the interpretation of the results, we intentionally work with a full network of 36 uncorrelated observations of the model variables placed at the model grid points, and affected by an error with standard deviation equal to 15% of the system natural variability. The observation operator is therefore inherently linear and coincides with the identity 36×36 matrix. The assimilation interval is fixed successively to 3, 6 and 12 h. All the experiments are performed in a perfect model scenario, but the parameter configurations are modified in order to analyse the filter behaviour in a range of different dynamical regimes. The configurations, which differ in the external forcing F, are reported in Table 1 along with some corresponding asymptotic stability properties computed over 20-yr-long simulations. We see that by increasing F the model becomes progressively more unstable; furthermore in configuration C_{sVI} the model solution is a stable periodic orbit with a period of approximately 400 h of simulated time. As described in Lorenz (1995) for sufficiently small F the system possess a 0-dimensional attractor at $x_1 = x_2 = \cdots = x_{36} = F$. To guarantee that the model trajectory is already on the system attractor, the initial conditions for all the OSSE experiments are obtained after 20-yr-long runs for each of the parameter configurations considered. The MLEF analysis cycle experiments last for 75 d. The first 15 d are considered to be a spin-up period so that the results that follow are computed over the last 60 d.

We study first the effect of chaotic dynamics on the information matrix in the ensemble space, $\mathbf{C}$. Figure 4 shows the spectrum of the eigenvalues of $\mathbf{C}$ when the model is employed in the canonical configuration C_0. The normalized distributions of the number of eigenvalues accounting for 50% (dashed lines), 90% (continuous line) and 99% (dotted lines) of the total explained variance is plotted. The distributions are built by computing and storing the relevant number of eigenvalues at each analysis time. From the left to the right the panels refer to experiments with $N_{\mathrm{ens}} = 6$, 18, 36, 54 and 72, respectively, while from above they refer to experiments with $\tau = 6$ and 12 h, respectively. The first remarkable feature is that a number of eigenvalues equal to less than half of the full phase space dimension appears sufficient to explain almost all the error variance. In practice, once the threshold value of $N_{\mathrm{ens}} = 18$ is passed, the matrix $\mathbf{C}$ and consequently the analysis increment, spans a subspace whose dimension, on average, does not seem to be sensible to the size of the ensemble and never exceeds 15. It is worth mentioning that this number is close to the number of positive Lyapunov exponents ($N_{\sigma^+} = 11$, Table 1). Given that the variance explained by the forecast ensemble members is neither increased by an inflating procedure nor by introducing noise at the analysis update, the matrix $\mathbf{P}^f$ reflects naturally the properties of the underlying dynamics such

Table 1. Summary of the model configurations used in the experiments with the associated instability properties

	F	$\sigma_{\max}$ (d)$^{-1}$	$\mathbf{N}_{\sigma+}$	**KY-dim**	$\mathbf{T}_2$(d)	**KS-ent**(d)$^{-1}$
C_{uI}	14.40	0.69	13	29.02	1.00	4.24
C_0	8.00	0.33	11	24.35	2.10	1.82
C_{sI}	6.40	0.21	10	21.17	3.30	1.09
C_{sII}	5.60	0.16	9	18.87	4.33	0.70
C_{sIII}	4.65	0.07	6	13.27	9.49	0.18
C_{sIV}	4.52	0.02	4	8.92	25.62	0.05
C_{sV}	4.50	0.004	2	5.03	173.28	0.004
C_{sVI}	2.00	Stable periodic orbit	–	–	–	–

Notes: The model configurations differ for the external forcing F (second column). The stability properties are (from the third to the last column): leading Lyapunov exponents $\sigma_{\max}$ expressed in d^{-1}, the number of positive Lyapunov exponents $\mathbf{N}_{\sigma+}$, the Kaplan–Yorke dimension **KY-dim**, the doubling time $\mathbf{T}_2$ expressed in day and the Kolmogorov–Sinai entropy, **KS-ent** expressed in d^{-1}. Results are based on a 20-yr-long integration.

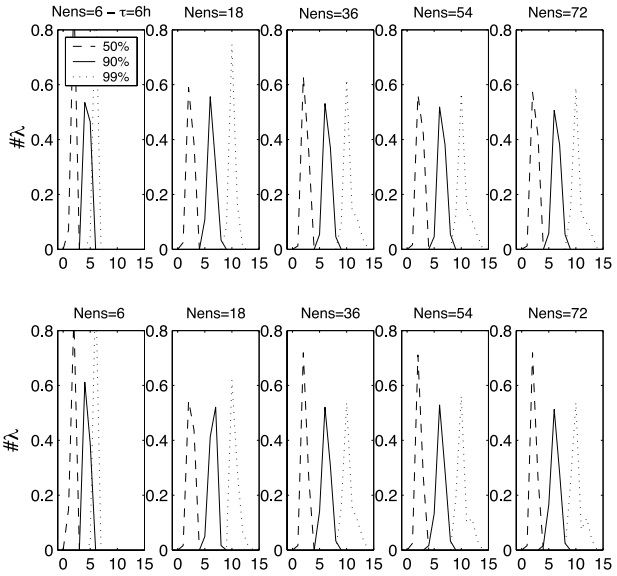

Fig. 4. Lorenz model. Normalized distributions of the eigenvalues of **C**, for different ensemble sizes—from the left to the right $N_{\text{ens}} = 6$, 18, 36, 54, 72—and for different assimilation interval—$\tau = 6$ h (top panels), $\tau = 12$ h (bottom panels). Number of eigenvalues accounting for 50% (dashed lines), 90% (continuous line) and 99% (dotted lines) of the total explained variance.

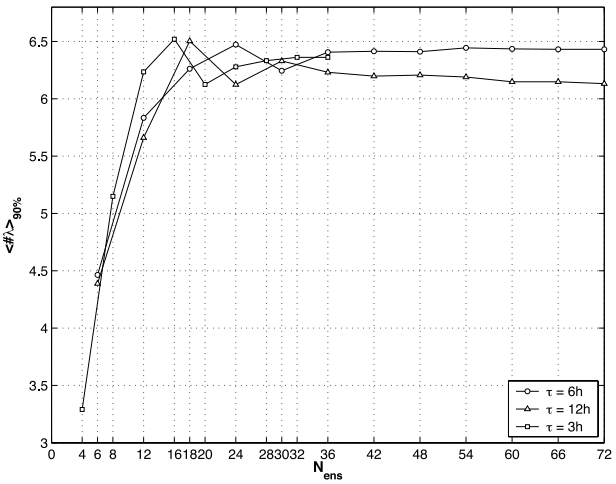

Fig. 5. Lorenz model. Mean number of eigenvalues accounting for 90% of the explained variance as a function of N_{ens} and for different assimilation interval—τ, 12 (triangles), 6 (circles) and 3 h (squares).

as the number of error growth directions. Note that none of those empirical techniques to optimize the variance explained by the ensemble has been so far necessary in applications with the MLEF. This choice is further motivated here by the need to have an experimental setup which makes the interpretation of the filter response to different dynamical regimes easier.

A complementary picture of this mechanism is highlighted in Fig. 5, where the mean number of eigenvalues accounting for 90% of the explained variance is shown as a function of N_{ens} and for different τ, 12 (triangles), 6 (circles) and 3 h (squares). The model is again in its canonical configuration. For all the assimilation intervals, when the value of $N_{\text{ens}} = 6 - 8$ is passed the number of eigenvalues jumps suddenly to a value of about 6. Thereafter the curves become almost flat (the same can be argued to happen for the case $\tau = 3$ h but the analysis does not include experiments with $N_{\text{ens}} > 36$). Note finally that when $N_{\text{ens}} \geq 36$ a progressively smaller number of eigenvalues is necessary to explain 90% of the variance when the assimilation interval is increased, as it can be deduced also from Fig. 4. This feature is probably due to the convergence of the ensemble subspace to the system's unstable subspace. The convergence takes place at

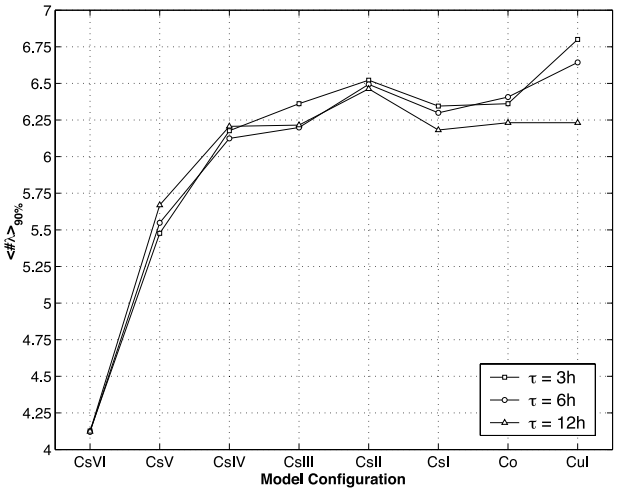

Fig. 6. Lorenz model. Mean number of eigenvalues explaining 90% of the variance as a function of the model configuration and for different assimilation interval—τ, 12 (triangles), 6 (circles) and 3 h (squares). In all the experiments $N_{\text{ens}} = 36$.

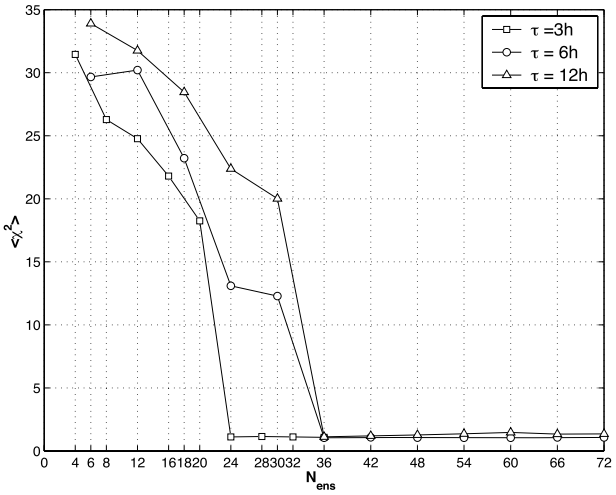

Fig. 7. Lorenz model. Mean χ^2, $\langle\chi^2\rangle$ (along the complete data assimilation cycle), with respect to N_{ens} and for different assimilation interval—τ, 12 (triangles), 6 (circles) and 3 h (squares).

a rate given by the dominant Lyapunov exponents. Therefore, for longer τ, this confinement is enhanced.

A similar analysis has been made for different model configurations and is summarized in Fig. 6, which shows the mean number of eigenvalues explaining 90% of the variance and for $\tau = 12$, 6 and 3 h, for $N_{\text{ens}} = 36$. The most remarkable feature is the increase of the number of eigenvalues for more unstable configurations, which may be related to the increase of the number of positive Lyapunov exponents. So the results of Fig. 6 support the interpretation given in relation to Fig. 4.

Note that in some cases a lower number of λ is sufficient even in correspondence of a more unstable configuration (compare C_{sI} with C_{sII}). Thus, the first conclusion one can draw is that the more unstable the model the larger is the subspace where errors are confined but the overall picture is not so clear and the presence of the fluctuations around an almost constant plateau suggests the role of additional factors, such as the natural variability of the local instabilities on the system's attractor.

An analysis (not shown) of the flow dependent character of the system instabilities has been made by computing the distributions of the 12 h growth rates (the finite time leading Lyapunov exponent), the local number of growing modes, the Kolmogorov–Sinai entropy (KS-ent, i.e. the sum of the positive Lyapunov exponents, $\mathbf{KS\text{-}ent} = \sum_{i=1}^{N_{\sigma^+}} \sigma_i$), and the Lyapunov or Kaplan–Yorke dimension ($KY - dim$) characterizing the dimension of the volumes conserved, on average, along the flow (Kaplan and Yorke, 1979), for the model (19) in the canonical configuration C_0 and on the base of 20-yr-long experiments. Note that the Kaplan-Yorke dimension is closely related to other concepts of dimensions known in the literature (Ott, 2002). It is defined as $KY - dim = d^- + \frac{\sum_{i=1}^{d^-} \sigma_i}{|\sigma_{d^+}|}$, where d^- is the largest number of Lyapunov exponents for which the summation, $\sum_{i=1}^{d^-} \sigma_i$, is positive and d^+ is the smallest number of Lyapunov exponents for which the summation is negative.

All these quantities can be seen as a measure of the average instability of the system. Local instabilities are characterized by large distributions whose standard deviations closely approach the mean values, indicating that situations relatively stable alternate with others much more unstable. This represents a hard challenge for the filter which should be able to properly account for the system instabilities and to track the true state. The mean values of all these quantities and for all the model configurations are given in Table 1.

Coming back to Fig. 6, the three configurations (C_{sII}, C_{sI} and C_0) are quite close to each other in terms of their asymptotic properties. We can thus interpret the results on the mean number of eigenvalues in relation with the local variability of the Lyapunov exponents.

We now turn to the analysis of the filter performance using the χ^2 test of the innovations. From the classical Kalman filter theory (for linear systems and observation operators), it is known that, in the hypothesis that the forecast and observation errors are Gaussian and uncorrelated in time, the innovations are also Gaussian (Jazwinski, 1970). As a consequence, studying the distribution of innovations results in a test on the underlying assumptions of Gaussian and time uncorrelated errors. Here we consider the normalized innovations that, under the aforementioned hypothesis, are distributed according to $\mathcal{N}(0, 1)$ (Reichle et al., 2002), computed along the MLEF solution for different ensemble sizes. Under these conditions, the χ^2 test of the squared normalized innovations should have a conditional mean equal to one. Furthermore, since in the experiments here the observations are mutually uncorrelated and uncorrelated in time, the χ^2 statistics turns out to be a verification tool for the forecast error covariance $\mathbf{P}_f^{1/2}$. A χ^2 mean larger than one ($\langle\chi^2\rangle > 1$)

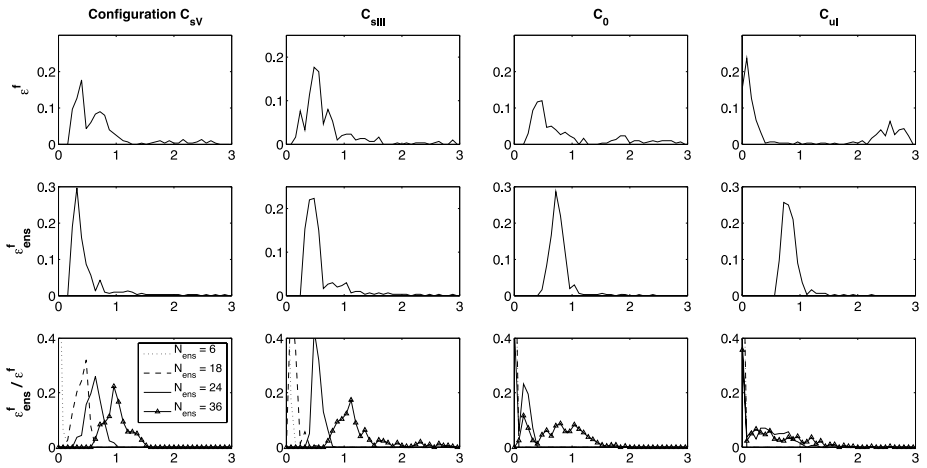

Fig. 8. Lorenz model. Top plots: distribution of the 6 h actual rms forecast error, ϵ^f, for the configurations C_{sV}, C_{sIII}, C_0 and C_{uI}, with $N_{\rm ens} = 36$. Middle plots: distribution of the ensemble based estimate of the rms forecast error, $\epsilon^f_{\rm ens}$, for the same configurations and $N_{\rm ens}$. Bottom plots: distribution of the ratio $\epsilon^f_{\rm ens}/\epsilon^f$ for the same configurations and for $N_{\rm ens} = 6$, 18, 24 and 36. All error are normalized with respect to the system's natural variability.

indicates underestimation of the actual forecast error covariance, and the opposite for a χ^2 mean less than one (see Zupanski and Zupanski, 2006, for more details). Figure 7 shows the χ^2 mean, $\langle\chi^2\rangle$ (along the complete data assimilation cycle), with respect to $N_{\rm ens}$ for the model in the canonical configuration and τ equal to 3, 6 and 12 h. In all the experiments, as long as $N_{\rm ens} < 36$, $\langle\chi^2\rangle$ remains larger than 1, indicating that the actual error is underestimated by the ensemble. As $N_{\rm ens}$ is increased towards $N_{\rm ens} = 36$, $\langle\chi^2\rangle$ decreases monotonically. The convergence to small values is clearly different among the experiments and the strength of the observational forcing (in terms of the observation frequency) affects this convergence. Close to $N_{\rm ens} = 36$ $\langle\chi^2\rangle$ drops dramatically (for $\tau = 3$, $\langle\chi^2\rangle$ starts to drop significantly by $N_{\rm ens} = 24$). Once the optimal value $\langle\chi^2\rangle = 1.00$ is reached in the proximity of $N_{\rm ens} = 36$, it remains approximately constant even when a larger ensemble is used. This is different from stochastic filters where the quality of the ensemble based statistics improves as the sample (i.e. the ensemble) size increases.

The ability of the ensemble to accurately describe the actual forecast error is further analysed in Fig. 8. In the top row of the figure are plotted the distributions of the 6 h rms forecast error, ϵ^f, in the MLEF analysis cycles with $N_{\rm ens} = 36$. Four typical model configurations are examined and are indicated in the corresponding plots. In the second row are shown the distributions of the rms forecast error estimated by the ensemble, $\epsilon^f_{\rm ens}$. At the bottom, it is shown the distribution of the ratio $\epsilon^f_{\rm ens}/\epsilon^f$ for $N_{\rm ens} = 6$, 18, 24 and 36. To facilitate the interpretation, all errors are normalized with respect to the system's natural variability.

The distributions of ϵ^f immediately reveal the non-Gaussian character of the errors. The distributions do not display unimodality and in the most unstable configuration, C_{uI}, a bimodal shape appears. Remarkably the distributions of the estimated error, $\epsilon^f_{\rm ens}$, for the configurations C_{sV}, C_{sIII} and C_0 are very similar to those of ϵ^f. In particular they capture their most populated peak. On the other hand, in the configuration C_{uI}, the ensemble based estimate appears less accurate. It does not reproduce the almost bimodal shape of the distribution of ϵ^f and its peak is centered where the distribution of ϵ^f is sparsely populated. Another picture of the MLEF ensemble accuracy is given by the distributions of the ratio $\epsilon^f_{\rm ens}/\epsilon^f$, which allow to visualize the frequency of under/over error estimation. By plotting the curves for different $N_{\rm ens}$ we can observe their shift towards larger values when $N_{\rm ens}$ is increased. In the configurations C_{sV} and C_{sIII} the distributions for $N_{\rm ens} = 36$ are well centred around one as desired. In the case C_0 and for $N_{\rm ens} < 36$, the MLEF ensemble strongly underestimate the actual forecast error; for $N_{\rm ens} = 36$ the distribution has a peak close to one but it is characterized by a large standard deviation indicating that the ensemble is often underestimating ϵ^f. As expected the situation deteriorates further in the configuration C_{uI} where an almost systematic under estimation of error is observed. This different behaviour of the MLEF with dynamics of increasing instability is confirmed by the study of the rms analysis error provided in Fig. 9. A conclusion which can be drawn by this analysis is that an assimilation algorithm based on the maximum likelihood approach, applied to a chaotic system, may provide satisfactory results as long as the degree of instabilities do not induce strong departures from unimodality. These questions should be further explored in the future through the use of non-Gaussian filters. The artificial inflation of the forecast ensemble may counteract the error underestimation in the directions spanned by the ensemble. Anyhow it is expected to have scarce effect if the ensemble is not capturing all the relevant directions of error growth, as it can occur in the presence of non-linearities. A localization procedure, such as in

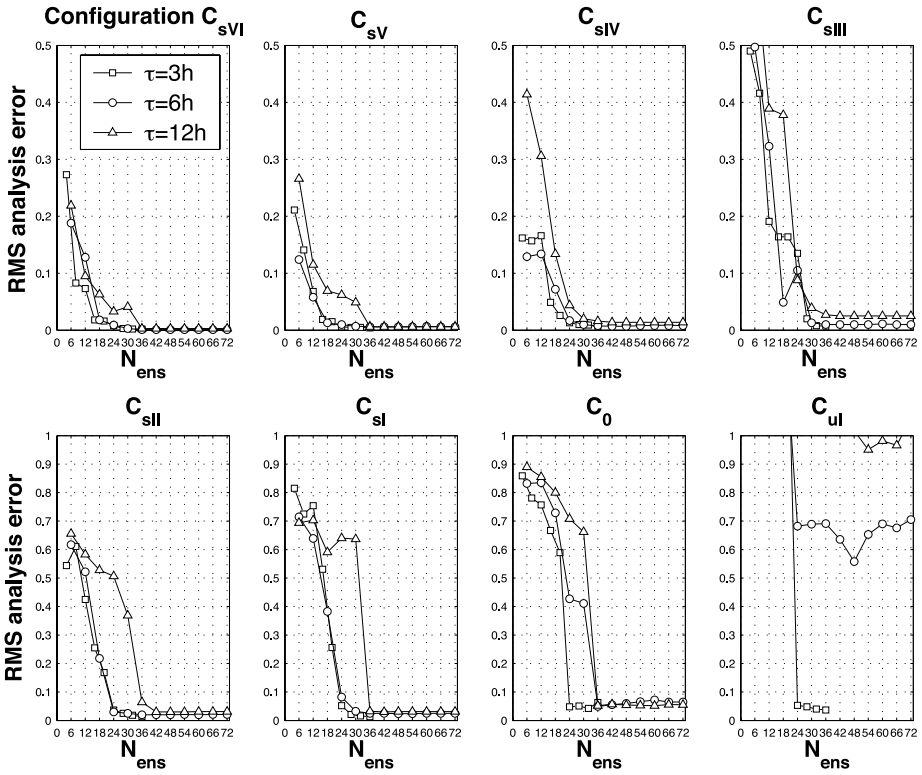

Fig. 9. Lorenz model. RMS analysis error as a function of N_{ens} for all the model configuration considered and for different assimilation interval — τ, 12 (triangles), 6 (circles) and 3 h (squares).

Ott et al. (2004), may be more efficient in those cases. In previous applications of the MLEF with complex models possessing many degrees of freedom, a covariance localization has been successfully applied and helps maintaining a sufficient number of the degrees of freedom in the data assimilation system (e.g. Zupanski, 2009).

The next step in our analysis is the investigation of the filter ability to produce accurate estimate of the unknown true system. The most natural way to accomplish this task is to evaluate the root-mean-square (rms) analysis error as a function of the ensemble size. In Fig. 9 the rms analysis error as a function of N_{ens} for all the model configuration considered, is shown. The overall picture is similar to the results shown in Fig. 7. The panels are ordered so that, from the top left- to bottom right-hand panels, they refer to progressively more unstable configurations. Note that two different scales are adopted for the y-axis between the top and bottom panels. As expected, better results (lower error level) are obtained for more stable configurations, and/or for shorter τ. Note that in the most unstable configuration, C_{uI}, the convergence is obtained only for small assimilation time scale ($\tau = 3$ h) and that even in the case of the stable periodic orbit, configuration C_{sVI}, at least six members are necessary to reduce the error below the observation level. We see that once a given threshold value for N_{ens} is reached no further improvements of the filter are obtained. The situation is closely related to what is observed in Section 3 for the scalar and the saddle node examples. In particular in the latter case, increasing N_{ens} beyond $N_{\text{ens}} = 1$ (the number of unstable modes) did not lead to any further improvement of the filter performance. We argue that the same underlying mechanism is occurring here and that this convergence value for N_{ens} is related to the system stability properties. In a recent study, Sakov and Oke (2008) observed a similar behaviour in relation to the ensemble size in the context of the Ensemble Transform Kalman filter (Bishop et al., 2001).

This aspect is further highlighted in Fig. 10. In the abscissa the Kaplan–Yorke attractor dimension for all the model configurations is plotted, while N_{ens} is given in the y-axis. The points in the figure are obtained by considering, for each model configuration, the first (minimum) value of N_{ens} for which the rms analysis error is smaller or equal to 10% of the system's natural variability. We consider the values of N_{ens} given in Fig. 10 as 'optimal' because they represent a compromise between the filter performance and the computational constraints (i.e. the number of members). We see that in most of the cases, the error reduction to 10% of the natural variability is reached as soon as N_{ens} passes the KY-dim of the system; this is particularly evident in correspondence with the strongest observational forcing ($\tau = 3$ h). The KY-dim is defined only for chaotic dynamics, and the results of the stable configuration C_{sVI} (in the figure indicated as KY-dim = 0) are plotted for reasons of completness.

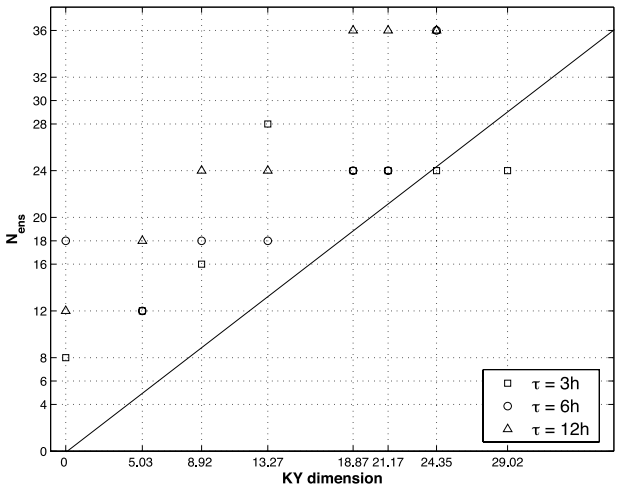

Fig. 10. Lorenz model. *Optimal* N_{ens} (see text) as a function of the Kaplan–Yorke dimension of each model configuration and for different assimilation interval—τ, 12 (triangles), 6 (circles) and 3 h (squares).

Although in some case a larger N_{ens} is found in correspondence of stabler configurations (i.e. smaller KY-dim) or a same N_{ens} for model configurations characterized by different KY-dimensions, the overall picture of Fig. 10 suggests the existence of a fuzzy link between the system dynamical properties and the size the MLEF ensemble necessary to properly explain and track the error variance in the state estimate. Note that the same relation may be observed by looking at other measures of the system stability properties such as the number of positive Lyapunov exponents or the Kolmogorov–Sinai entropy; see Table 1. For the system considered here, these latter quantities appear of lesser practical use than the KY-dim which on the other hand provides a lower limit (i.e. a necessary condition) for an adequate ensemble size. A rough estimate of the adequate ensemble size would be here of the order of twice the attractor dimension (or the phase space dimension for larger KY-dim). This feature probably reflects the inhomogeneity of the attractor (variability of the local instabilities) which implies the presence of dynamical situations for which the local unstable subspace dimension is larger than the average KY-dim.

It is worth to note that the results of Fig. 10 show a somewhat similar trend to the eigenvalues spectrum of **C** given in Fig. 5. A growing interval followed by a small oscillatory period and finally an almost stable value. This points out to a possible link between the eigenvalue spectrum of **C** and the KY-dim. Finally, according to the EVD analysis, one would expect that a limited number of directions is sufficient, on average, to explain most of the variance of the error (15 for 90%). On the other hand, we see that a satisfactory filter performance is obtained only for N_{ens} closer to the system attractor dimension. To explain this difference one must realize that the spectral properties of the matrix **C** reflect the ability of the assimilation in reducing the error variance as given in $\mathbf{P}_f$ at the times of the analysis, while the optimal N_{ens} gives the size the ensemble should have to provide, on average, an adequate description of the actual error variance before the assimilation of the observations. These quantities reveal therefore complementary aspects of the assimilation process.

5. Conclusion

Data assimilation developments have been long faced to chaotic dynamics. The state estimation problem for this class of systems is particularly important realizing that chaotic behaviour is present in most of the natural systems, including the atmosphere and ocean. The MLEF has proved to be an efficient data assimilation technique and to be able to provide accurate track of the system state in several applications from idealized low-dimensional systems up to almost operational NWP models. It belongs to the large class of the so called ensemble based scheme, although it has a number of essential features shared with variational algorithms. This study was motivated by the lack of an extensive analysis of the MLEF in the context of chaotic unstable dynamics.

When applied to the two generic dynamics produced by a scalar unstable system and by the saddle point, it was found that no benefit is gained in the filter performance when the ensemble size is larger than one, corresponding to the number of unstable modes in both systems. In addition, the algorithm operates an implicit normalization with the effect of a re-distribution of the explained variance among the ensemble members.

The filter has then been analysed by performing observation system simulation experiments in the context of the 36-variable Lorenz system. The model has been employed in a set of different parameter configurations whose solutions exhibit a range of regimes of motion from stable periodic orbit to highly chaotic behaviour. First, the properties of the ensemble information matrix **C** have been analysed with respect to the ensemble size and to the model configuration. Interestingly, for the canonical model configuration (a chaotic one), by increasing the ensemble size, the number of its relevant eigenvalues rapidly attained a limit value of about 6. In particular, the results do not show significant modifications in the spectral properties of **C** once an ensemble of at least 18 members is used. A similar behaviour of the spectral properties of **C** is found in all the other unstable model configurations considered (not shown). When the same analysis is performed with respect to the model configurations and with a fixed ensemble size, the number of relevant eigenvalues increases when more unstable configurations are considered.

The accuracy of the filter ensemble based statistics has been then studied in relation to the ensemble size and model configurations, by analysing the statistics of the normalized innovations. The results clearly show that, as expected, by increasing the ensemble size a progressively better error description is provided, but also that this improvement reaches saturation in correspondence to an ensemble size closely related to the system's attractor

dimension and bounded to the system state dimension. The rms analysis error exhibits a similar trend. The existence of a saturation value for the ensemble size is confirmed. Repeating the same analysis for all the model configurations, revealed that this saturation level increases according to the level of instabilities of the model, bounded to the full system phase space dimension.

The link between the optimal ensemble size and the system stability properties is reflected by its relation with the Kaplan–Yorke attractor dimension. A conjecture establishes the equivalence between the Kaplan–Yorke and the information dimension (Ott, 2002), which characterizes the dimension of the attractor based on its natural measure (the invariant probability distribution). In addition, the Kaplan–Yorke dimension is commonly seen as the dimension of volumes which are conserved under the action of system's flow. We can thus speculate that the ensemble perturbations in the MLEF feature the intrinsic system error dynamics, and not a set of realizations of a Monte Carlo sampling as for the ensemble Kalman filter. This finding may help guiding the setup of the filter for applications to chaotic dynamics, by choosing an ensemble size larger than the system attractor dimension which is, for typical dissipative systems as the ones used in atmospheric and oceanic models, much less than the full phase space dimension.

We are currently working on the extension of the present analysis based on the MLEF to chaotic systems in which model error is present, in the spirit of a recent paper on the reassessment of the extended KF in the presence of deterministic model errors (Carrassi et al., 2008b). The formulation proposed in that study is based on fundamental findings on the dynamics of deterministic model errors (Nicolis, 2003; Nicolis et al., 2009). The extension to the MLEF appears thus a natural step ahead in the timely subject of model error in ensemble filters.

6. Acknowledgments

The authors wish to thank Prof. Catherine Nicolis for the careful reading of the manuscript and the three anonymous Reviewers for their insightful comments which help improving the original version of the manuscript. This work was supported by the Belgian Federal Science Policy Program under contract MO/34/017.

7. Appendix

Let us consider the saddle node system (16) and the MLEF with a 2-members ensemble and two uncorrelated noisy observations, $\mathbf{x}_o = (x_{o,1}, x_{o,2})$. The square-root forecast error covariance and the observation error covariance matrices can be written as

$$\mathbf{P}_f^{1/2} = \begin{pmatrix} \sigma_{f,11} & \sigma_{f,21} \\ \sigma_{f,12} & \sigma_{f,22} \end{pmatrix} \qquad \mathbf{R} = \begin{pmatrix} \sigma_{o,1}^2 & 0 \\ 0 & \sigma_{o,2}^2 \end{pmatrix}.$$

In this example the observation operator, which is linear, coincides with the identity matrix in the bi-dimensional space. We can thus obtain for the information matrix $\mathbf{C}$

$$\mathbf{C} = \begin{pmatrix} \left(\sigma_{f,11}^2/\sigma_{o,1}^2\right) + \left(\sigma_{f,12}^2/\sigma_{o,2}^2\right) & \left(\sigma_{f,11}\sigma_{f,21}/\sigma_{o,1}^2\right) + \left(\sigma_{f,12}\sigma_{f,22}/\sigma_{o,2}^2\right) \\ \left(\sigma_{f,11}\sigma_{f,21}/\sigma_{o,1}^2\right) + \left(\sigma_{f,12}\sigma_{f,22}/\sigma_{o,2}^2\right) & \left(\sigma_{f,21}^2/\sigma_{o,1}^2\right) + \left(\sigma_{f,22}^2/\sigma_{o,2}^2\right) \end{pmatrix}.$$

Let indicate the two eigenvectors of $\mathbf{C}$ as $\mathbf{v}_1 = (v_{11}, v_{12})^T$ and $\mathbf{v}_2 = (v_{21}, v_{22})^T$, and the corresponding eigenvalues as λ_1 and λ_2, respectively. Therefore, for the transformation and precondition matrix we have

$$(\mathbf{I}+\mathbf{C})^{-1/2} = \begin{pmatrix} v_{11}^2/(1+\lambda_1)^{1/2} + v_{21}^2/(1+\lambda_2)^{1/2} & v_{11}v_{12}/(1+\lambda_1)^{1/2} + v_{21}v_{22}/(1+\lambda_2)^{1/2} \\ v_{11}v_{12}/(1+\lambda_1)^{1/2} + v_{21}v_{22}/(1+\lambda_2)^{1/2} & v_{12}^2/(1+\lambda_1)^{1/2} + v_{22}^2/(1+\lambda_2)^{1/2} \end{pmatrix}.$$

Introducing the control variable $\mathbf{x} - \mathbf{x}_f = \mathbf{P}_f^{1/2}(\mathbf{I}+\mathbf{C})^{-T/2}\boldsymbol{\xi}$, $\boldsymbol{\xi} = (\xi_1, \xi_2)^T$, we can now write the cost-function in the ensemble subspace

$$2J(\boldsymbol{\xi}) = \boldsymbol{\xi}^T(\mathbf{I}+\mathbf{C})^{-1}\boldsymbol{\xi} + \left[\mathbf{x}_o - \mathbf{x}_f - \mathbf{P}_f^{1/2}(\mathbf{I}+\mathbf{C})^{-1/2}\boldsymbol{\xi}\right]^T \mathbf{R}^{-1} \left[\mathbf{x}_o - \mathbf{x}_f - \mathbf{P}_f^{1/2}(\mathbf{I}+\mathbf{C})^{-1/2}\boldsymbol{\xi}\right].$$

The cost-function minimum is obtained by solving a linear system of two equations resulting from the condition of gradient equal to zero

$$\nabla_{\boldsymbol{\xi}} J(\boldsymbol{\xi}) = 0 \Leftrightarrow \begin{cases} \frac{\partial J}{\partial \xi_1} = 0 \\ \frac{\partial J}{\partial \xi_2} = 0. \end{cases}$$

If the solution, $\overline{\xi}$, verifies also the condition $\nabla^2 J(\overline{\xi}) > 0$, we have $\xi_{opt} = \overline{\xi}$, the optimal solution.Finally, the analysis in the original system phase space reads:

$$\mathbf{x}_a = \mathbf{x}_f + \mathbf{P}_f^{1/2}(\mathbf{I}+\mathbf{C})^{-T/2}\xi_{\text{opt}}$$

while the analysis error covariance update

$$\mathbf{P}_a^{1/2} = \mathbf{P}_f^{1/2}(\mathbf{I}+\mathbf{C})^{-1/2}$$

and the cycle can be repeated.

References

Anderson, J. L. 2001. An ensemble adjustment Kalman filter for data assimilation. *Mon. Wea. Rev.* **129**, 2884–2903.

Bishop, C., Etherton, J. and Majumdar, S. J. 2001. Adaptive sampling with the ensemble transform Kalman filter. Part I: theoretical aspects. *Mon. Wea. Rev.* **129**, 420–436.

Carrassi, A., Ghil, M., Trevisan, A. and Uboldi, F. 2008a. Data assimilation as a nonlinear dynamical system problem: stability and convergence of the prediction-assimilation system. *Chaos* **18**, 023112.

Carrassi, A., Vannitsem, S. and Nicolis, C. 2008b. Model error and sequential data assimilation: a deterministic formulation. *Q. J. R. Meterol. Soc.* **134**, 1297–1313.

Carrio, G. G., Cotton, W. R., Zupanski, D. and Zupanski, M. 2008. Development of an aerosol retrieval method: description and preliminary tests. *J. Appl. Meteorol. Climatol.* **47**, 2760–2776

Evensen, G. 1994. Sequential data assimilation with a nonlinear quasi-geostrophic model using Monte-Carlo methods to forecast error statistics. *J. Geophys. Res.* **99**(C5), 10 143–10 162.

Fletcher, S. J. and Zupanski, M. 2006a. A data assimilation method for lognormally distributed observation errors. *Q. J. R. Meteorol. Soc.* **132**, 2505–2520.

Fletcher, S. J. and Zupanski, M. 2006b. A hybrid multivariate normal and lognormal distribution for data assimilation. *Atmos. Sci. Let.* **7**, 43–46.

Fletcher, S. J. and Zupanski, M. 2008. Implications and impacts of transforming lognormal variables into normal variables in VAR. *Met. Zeit.* **16**, 755–765.

Ghil, M. 1997. Advances in sequential estimation for atmospheric and oceanic flows. *J. Meteorol. Soc. Jpn.* **75**, 289–304.

Jazwinski, A. H. 1970. *Stochastic Processes and Filtering Theory*, Academic Press, London.

Heemink, A. W., Verlaan, M. and Segers, J. 2001. Variance reduced ensemble Kalman filtering. *Mon. Wea. Rev.* **129**, 1718–1728.

Houtekamer, P. L. and Mitchell, H. L. 1998. Data assimilation using an ensemble Kalman filter technique. *Mon. Wea. Rev.* **126**, 796–811.

Kalman, R. 1960. A new approach to linear filtering and prediction problems. *Trans. ASME, J. Basic Eng.* **82**, 35–45.

Kalnay, E. 2003. *Atmospheric Modeling, Data Assimilation and Predictability*, Cambridge University Press, Cambridge.

Kaplan, J. L. and Yorke, J. A. 1979. Chaotic behavior of multidimensional difference equations. In: *Functional Differential Equations and Approximations of Fixed Points* (eds H.-O. Peitgen and H.-O. Walter). Lecture Notes in Mathematics, Vol. 730. Springer, Berlin, p. 204.

Lawson, W. G. and Hansen, J. A. 2004. Implications of stochastic and deterministic filters as ensemble-based data assimilation methods in varying regimes of error growth. *Mon. Wea. Rev.* **132**, 1966–1981.

Lorenc, A. C. 1986. Analysis methods for numerical weather prediction. *Q. J. R. Meteorol. Soc.* **112**, 1177–1194.

Lorenz, E. N. 1995. 'Predictability: a problem partly solved'. *Proc. Seminar on Predictability*, Vol. 1, Reading, UK, ECMWF, 1–18.

Nicolis, C. 2003. Dynamics of model error: some generic features. *J. Atmos. Sci.* **60**, 2208–2218.

Nicolis, C., Perdigao, R. and Vannitsem, S. 2009. Dynamics of prediction errors under the combined effect of initial condition and model errors. *J. Atmos. Sci.* **66**, 766–778.

Ott, E. 2002. *Chaos in Dynamical Systems*, Cambridge University Press, Cambridge.

Ott, E., Hunt, B. R., Szunyogh, I., Zimin, A. V., Kostelich, E. J. and co-authors. 2004. A Local Ensemble Kalman Filter for atmospheric data assimilation in oceanography. *Tellus* **56A**, 273–277.

Pham, D. T., Verron, J. and Roubaud, M. C. 1998. A singular evolutive extended Kalman filter for data assimilation in oceanography. *J. Marine Sys.* **16**, 323–340.

Reichle, R. H., Walker, J. P., Koster, R. D. and Houser, P. R. 2002. Extended versus ensemble Kalman filtering to land data assimilation. *J. Hydrometeor* **3**, 728–740.

Rozier, D., Birol, F., Cosme, E., Brasseur, P., Brankart, J. M. and co-authors. 2007. A reduced-order Kalman filter for data assimilation in physical oceanography. *SIAM Rev.* **49**, 449–465.

Sakov, P. and Oke, P. R. 2008. Implications of the Form of the ensemble transformation in the ensemble square root filters. *Mon. Wea. Rev.* **136**, 1042–1053.

Tippet, M. K., Anderson, J. L., Bishop, C. H., Hamill, T. M. and Whitaker, J. S. 2003. Ensemble square root filters. *Mon. Wea. Rev.* **131**, 1490–113.

Trevisan, A. and Uboldi, F. 2004. Assimilation of Standard and targeted observations within the unstable subspace of the observation-analysis-forecast cycle system. *J. Atmos. Sci.* **61**, 103–113.

Uzunoglu, B., Fletcher, S. J., Zupanski, M. and Navon, I. M. 2007. Adaptive ensemble size inflation and reduction. *Q. J. R. Meteorol. Soc.* **133**, 1281–1294.

Whitaker, J. S. and Hamill, T. M. 2002. Ensemble data assimilation without perturbed observations. *Mon. Wea. Rev.* **130**, 1913–1924.

Zupanski, M. 2005. Maximum likelihood ensemble filter: theoretical aspects. *Mon. Wea. Rev.* **133**, 1710–1726.

Zupanski, D., 2009. Information measures in ensemble data assimilation. Chapter in the book. In: *Data Assimilation for Atmospheric, Oceanic, and Hydrologic Applications* (eds S. K. Park and L. Xu), Springer-Verlag, Berlin-Heidelberg. pp. 85–95, 475pp.

Zupanski, D. and Zupanski, M. 2006. Model error estimation employing an ensemble data assimilation approach. *Mon. Wea. Rev.* **134**, 1337–1354.

Zupanski, M., Fletcher, S. F., Navon, I. M., Uzunoglu, B., Heikes, R. P. and co-authors. 2006. Initiation of ensemble data assimilation. *Tellus* **58A**, 159–170.

Zupanski, D., Hou, A. Y., Zangh, S. Q., Zupanski, M., Kummerow, C. D. and co-authors. 2007a. Application of information theory in ensemble data assimilation. *Q. J. R. Meteorol. Soc.* **133**, 1533–1545.

Zupanski, D., Denning, A. S., Uliasz, M., Zupanski, M., Schuh, A. E. and co-authors. 2007b. Carbon flux bias estimation employing Maximum Likelihood Ensemble Filter (MLEF). *J. Geophys. Res.* **112**, D17107.

Zupanski, M., Navon, I. M. and Zupanski, D. 2008. The Maximum Likelihood Ensemble Filter as a non-differentiable minimization algorithm. *Quart. J. Roy. Meteorol. Soc.* **134**, 1039–1050.